

OPTICAL LOGICAL ELEMENTS

PACS numbers: 42.79.Ta; 42.65.Ky; 42.55.Px
DOI: 10.1070/QE2013v043n02ABEH014855

Demonstration and optimisation of an ultrafast all-optical AND logic gate using four-wave mixing in a semiconductor optical amplifier

M. Razaghi, A. Nosratpour, N.K. Das

Abstract. **We have proposed an all-optical AND logic gate based on four-wave mixing (FWM) in a semiconductor optical amplifier (SOA) integrated with an optical filter. In the scheme proposed, the preferred logical function can be performed without using a continuous-wave (cw) signal. The modified nonlinear Schrödinger equation (MNLSE) is used for the modelling wave propagation in a SOA. The MNLSE takes into account all nonlinear effects relevant to pico- and sub-picosecond pulse durations and is solved by the finite-difference beam-propagation method (FD-BPM). Based on the simulation results, the optimal output signal with a 40-fJ energy can be obtained at a bit rate of 50 Gb s^{-1}. In the simulations, besides the nonlinearities included in the model, the pattern effect of the signals propagating in the SOA medium and the effect of the input signal bit rate are extensively investigated to optimise the system performance.**

Keywords: *optical logic gate, semiconductor optical amplifier, four wave mixing, nonlinear effects, finite-difference beam-propagation method, pattern effect, bit rate.*

1. Introduction

High-speed all-optical logic gates are key elements in optical networks. Among these logic gates the all-optical AND gate is an important logic unit for optical communications. All-optical logic gates are based on nonlinear effects in a semiconductor optical amplifier (SOA), such as cross-gain modulation (XGM), cross-phase modulation (XPM), four-wave mixing (FWM), and cross-polarisation modulation (XPolM).

In recent years, various schemes for an optical AND gate with a various output bit rate have been proposed by using the XGM (10 Gb s^{-1}) [1], XPolM (10 Gb s^{-1}) [2], SOA-based Mach–Zehnder interferometer (SOA-MZI) (80 Gb s^{-1}) [3], SOA assisted by an optical filter (10 Gb s^{-1}) [4], FWM (5 Gb s^{-1}) [5], FWM with polarisation-shift-keying (PolSK) modulated signals (40 Gb s^{-1}) [6], cascaded single-port-coupled SOAs (10 Gb s^{-1}) [7], cascaded SOAs and optical filters (40 Gb s^{-1}) [8], SOA nonlinear polarisation rotation effect (10 Gb s^{-1}) [9], and semiconductor microresonators (30 Gb s^{-1}) [10].

M. Razaghi Department of Electrical and Computer Engineering, University of Kurdistan, Iran; e-mail: m.razaghi@uok.ac.ir;
A. Nosratpour Department of Electrical Engineering, Sanandaj Branch, Islamic Azad University, Sanandaj, Iran;
N.K. Das Department of Electrical and Computer Engineering, Curtin University, Perth, WA 6845, Australia

Received 25 March 2012; revision received 7 July 2012
Kvantovaya Elektronika **43** (2) 184–187 (2013)
Submitted in English

In this paper, to the best of our knowledge, for the first time a simple scheme for an all-optical AND logic gate using FWM in a SOA is investigated and optimised for high-speed optical communication systems (50-Gb s^{-1} output bit rate) which is compared with the previous published results (see, e.g., [5], where the scheme presented is a very complicated). The proposed scheme is significantly reasonable and easy to implement. For the proposed scheme, two data streams are simultaneously injected into the SOA while an additional cw signal is not required. The output signal (AND function) is achieved using an ideal filter with 1-THz bandwidth. In our scheme, all nonlinear effects, such as carrier depletion (CD), carrier heating (CH), spectral hole burning (SHB), group velocity dispersion (GVD), self-phase modulation (SPM), and two-photon absorption (TPA) are included in the SOA. The modified nonlinear Schrödinger equation (MNLSE) is used for the modelling wave propagation in a SOA [11, 12]. This MNLSE is solved by the finite-difference beam-propagation method (FD-BPM) [12, 13]. The BPM is widely used for the analysis of the field distribution in optical waveguides and optical pulse propagation in fibres. Based on the simulation time and results, we used the FD-BPM, because of short convergence time and excellent accuracy of the results [12–15].

2. Optical logic gate configuration

Figure 1 shows an AND logic gate operating on two serial optical return-to-zero (RZ) input signals 1 and 2, which are the input pump and probe signals, respectively. When two data streams (input signals) at different centre frequencies f_p (pump) and f_q (probe) are injected into a SOA simultaneously, the FWM signal is generated in the SOA at a frequency of $2f_p - f_q$, which is equivalent to the logic AND operation between the two input signals. Only if both input signals are present, then the FWM signal is generated (which is equal to the logic one '1'), and in other regimes the FWM signal is not generated (which is equal to logic zero '0', i.e., there is no output signal).

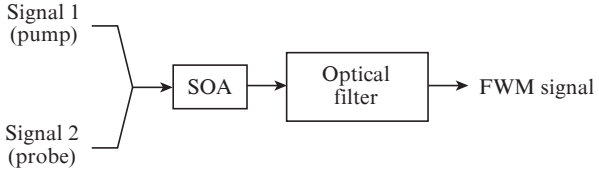

Figure 1. Schematic diagram of an AND gate.

3. Theory of the model

The model we have used for simulation of the SOA to obtain the logic gate is based on the MNLSE, which describes propagation of an optical pulse in the SOA using the slowly varying envelope approximation, i.e., under the assumption that the temporal change in the complex envelope function is very slow as compared with the optical field cycle [12].

$$\left[\frac{\partial}{\partial z} - \frac{\mathrm{i}}{2}\beta_2\frac{\partial^2}{\partial\tau^2} + \frac{\alpha_{\mathrm{int}}}{2} + \left(\frac{\gamma_{2\mathrm{p}}}{2} + \mathrm{i}b_2\right)\left|A(\tau,z)^2\right|\right]A(\tau,z)$$

$$= \left\{\frac{1}{2}g_N(\tau)\left[\frac{1}{f_T(\tau)} + \mathrm{i}\alpha_N\right] + \frac{1}{2}\Delta g_T(\tau)(1+\mathrm{i}\alpha_T)\right.$$

$$\left. -\mathrm{i}\frac{1}{2}\frac{\partial g(\tau,\omega)}{\partial\omega}\bigg|_{\omega_0}\frac{\partial}{\partial\tau} - \frac{1}{4}\frac{\partial^2 g(\tau,\omega)}{\partial\omega^2}\bigg|_{\omega_0}\frac{\partial^2}{\partial\tau^2}\right\}A(\tau,z), \qquad (1)$$

where $A(\tau,z)$ is the complex envelope function of an optical pulse; $|A(\tau,z)|^2$ is the optical pulse power; and τ is the frame of local time, which propagates with the group velocity v_{g} at the centre frequency of an optical pulse. Equation (1) makes use of the following notations and quantities:

$$g_N(t) = g_0\exp\left[-\frac{1}{E_{\mathrm{sat}}}\int_{-\infty}^{\infty}U(s)\exp\left(-\frac{s}{\tau_{\mathrm{s}}}\right)I(z,t-s)\,\mathrm{d}s\right]; \qquad (2)$$

$$f_T(t) = 1 + \frac{1}{\tau_{\mathrm{SHB}}P_{\mathrm{SHB}}}\int_{-\infty}^{\infty}U(s)\exp\left(-\frac{s}{\tau_{\mathrm{SHB}}}\right)I(z,t-s)\,\mathrm{d}s; \qquad (3)$$

$$\Delta g_T(t) =$$

$$-h_1\int_{-\infty}^{\infty}U(s)\exp\left(-\frac{s}{\tau_{\mathrm{CH}}}\right)\left[1-\exp\left(-\frac{s}{\tau_{\mathrm{SHB}}}\right)\right]I(z,t-s)\,\mathrm{d}s$$

$$-h_2\int_{-\infty}^{\infty}U(s)\exp\left(-\frac{s}{\tau_{\mathrm{CH}}}\right)\left[1-\exp\left(-\frac{s}{\tau_{\mathrm{SHB}}}\right)\right]I'(z,t-s)\,\mathrm{d}s; \qquad (4)$$

$$\frac{\partial g(t,\omega)}{\partial\omega}\bigg|_{\omega_0} = A_1 + B_1[g_0 - g(t,\omega_0)]; \qquad (5)$$

$$\frac{\partial^2 g(t,\omega)}{\partial\omega^2}\bigg|_{\omega_0} = A_2 + B_2[g_0 - g(t,\omega_0)]; \qquad (6)$$

$$g(t,\omega_0) = \frac{g_N(t,\omega_0)}{f_T(t)} + \Delta g_T(t,\omega_0); \qquad (7)$$

where β_2 is the GVD coefficient; α_{int} is the linear loss; $\gamma_{2\mathrm{p}}$ is the TPA coefficient; b_2 is the instantaneous SPM term due to the instantaneous nonlinear refractive index (Kerr effect); $g_N(t)$ is the saturated gain due to CD; g_0 is the linear gain; E_{sat} is the saturated energy; τ_{s} is the carrier lifetime; $f_T(t)$ is the SHB function; P_{SHB} is the SHB saturation power; τ_{SHB} is the spectral hole-burning relaxation time; α_N and α_T are the linewidth enhancement factors associated with the gain change due to CD and CH, respectively; $\Delta g_T(t)$ is the resulting gain change due to the CH and TPA; $U(s)$ is the unit step function; τ_{CH} is the CH relaxation time; h_1 is the contribution of stimulated emission and free-carrier absorption to CH gain reduction; h_2 is the contribution of TPA; A_1 and A_2 are the slope and curvature of the linear gain at ω_0, respectively; and B_1 and B_2 are the constants describing the changes in these quantities with saturation [12–15].

For solving Eqn (1), the SOA cavity is divided into M equal sections. By using a central-difference approximation in the time domain and trapezoidal integration over spatial section and applying an iterative procedure, a set of MNLSEs can be solved with high precision in a few seconds [12, 13].

4. Results and discussions

The parameters used in our simulations are listed in Table 1 [12]. In this simulation the envelope of input pulses corresponds to $\mathrm{sech}^2 x$. The full width at half maximum (FWHM) of the input pulses is 3.4 ps. The centre frequency of the pump pulse is 349 THz and the detuning frequency between the input pump and probe pulse, Δf, is 1 THz. Therefore, to separate the generated FWM signal, we have filtered the output signal spectrum (i.e., combined pump, probe and generated FWM signal) from –500 GHz to +500 GHz of the 350 THz (which is the FWM centre frequency) and performed the inverse Fourier transform of their respective components. In our simulations, the input pump and probe pulse energies are equal. Furthermore, the pattern effect (PE) is defined as the ratio of the maximum peak power ($P_{\max}$) to the minimum peak power ($P_{\min}$) of the generated FWM signal [16]:

$$\mathrm{PE} = 10\lg(P_{\max}/P_{\min}). \qquad (8)$$

The evolution of the generated FWM signal pulse train is shown in Fig. 2. Due to the gain recovery phenomena in the SOA, the initially generated FWM signal peak power is decreased with time. In Fig. 2a, when the long bit sequence of logic '1' occurs, the SOAs gain cannot recover to its initial value and remains constant for the rest of bits, and therefore, the FWM signal peak power is not changed. Figure 2b shows

Table 1. The parameters used in the simulations [12].

Parameter	Symbol	Value
SOA length	L	500 μm
Effective area	A_{r}	5 μm^2
Centre frequency of the pulse	f_0	349 THz
Saturation energy	E_{sat}	80 pJ
Linear gain	g_0	92 cm^{-1}
Group velocity dispersion	β_2	0.05 ps^2 cm^{-1}
Linewidth enhancement factor due to the carrier depletion	α_N	3.1
Linewidth enhancement factor due to the carrier heating	α_{CH}	2.0
Contribution of stimulated emission and free-carrier absorption to the carrier heating gain reduction	h_1	0.13 cm^{-1} pJ^{-1}
Contribution of two-photon absorption	h_2	126 fs cm^{-1} pJ^{-2}
Carrier lifetime	τ_{s}	200 ps
Carrier heating relaxation time	τ_{CH}	700 fs
Spectral-hole burning relaxation time	τ_{SHB}	60 fs
Spectral-hole burning relaxation power	P_{SHB}	28.3 W
Linear loss	α_{int}	11.5 cm^{-1}
Instantaneous nonlinear Kerr effect	n_2	–0.70 cm^2 TW^{-1}
Two-photon absorption coefficient	$\gamma_{2\mathrm{p}}$	1.1 cm^{-1} W^{-1}
Parameters describing second-order Taylor expansion of the dynamically gain spectrum	A_1	0.15 fs μm^{-1}
	B_1	–80 fs
	A_2	–60 fs^2 μm^{-1}
	B_2	0 fs^2

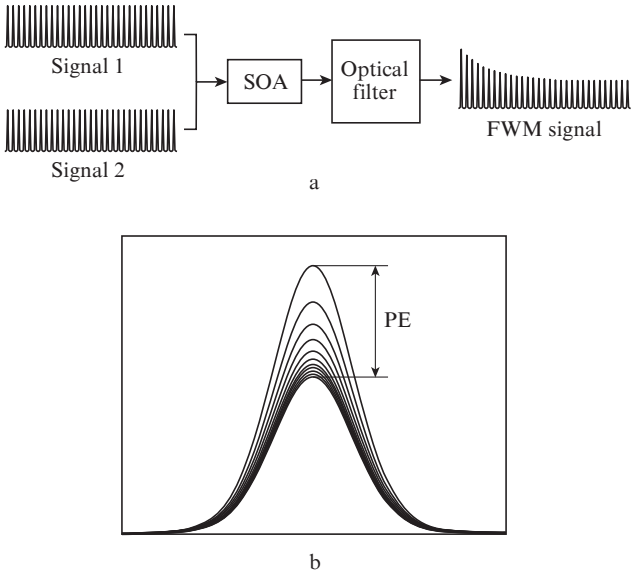

Figure 2. (a) SOA's output FWM signal for a long bit sequence of logic '1', and (b) eye diagram corresponding to the generated FWM signal as shown in Fig. 2a.

the eye diagram corresponding to the generated FWM signal as shown in Fig. 2a.

If due to the input signals, the SOA's output FWM signal becomes '0', the SOA regarding to the input bit sequence frequency may have sufficient time to recover to its initial value as shown in Fig. 3. One can see that for two input bit sequences '11111101' and '11111001', the AND logic operation is '11111001', the peak power of the generated FWM signal is reduced fast due to the gain recovery phenomenon.

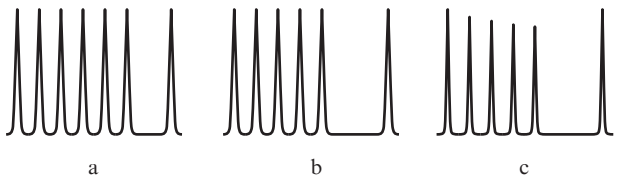

Figure 3. Illustrations of the SOA's gain recovery and demonstration of the PE: (a) signal 1, (b) signal 2, and (c) FWM signal.

Figure 4 shows the PE in the SOA for the generated FWM signal for various input pump and probe pulse energies. One can see that the PE increases for higher bit rates, which is due to the increase in the input signal frequency and the SOA does not have enough time to recover its gain to its initial value. Moreover, if the input signal energies increase, the carrier depletion effect becomes more powerful and the SOA requires more time to maintain the population inversion again and, therefore, the PE increases.

The bit rate of input pulses is 50 Gb s^{-1}, which makes our models results more applicable for the high-speed optical communication systems.

Figure 5 illustrates the PE in the SOA as a function of input pump and probe signal energies. When the low-energy input signals vary, the PE value changes significantly; however, when high-energy input signals (> 200 fJ) vary, the PE is saturated and does not change considerably. It should be

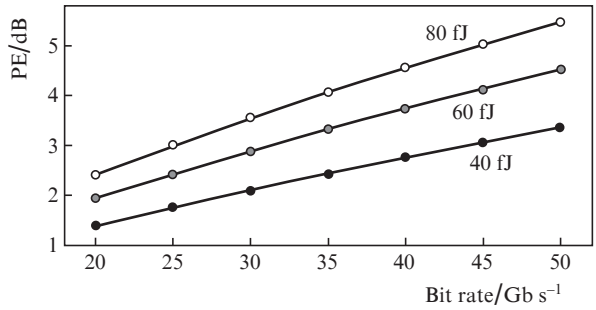

Figure 4. Pattern effect in the SOA for the generated FWM signal vs. the bit-rate characteristics for various input pump and probe signal energy levels.

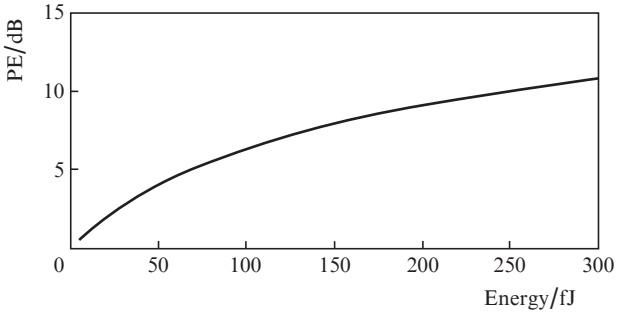

Figure 5. Pattern effect in the SOA for the FWM signal vs. the input pump/probe signal energy characteristics.

noted that for the optimum high-bit rate logic gate operation, the PE should be as low as possible and the input signal energy also should be chosen such that the desirable output FWM signal energy is generated.

Figure 6 shows the SOA gain variation as a function of the input signal energy. In this case, we have assumed that two input serial data with a long sequence of logic '1' bits is injected into the SOA. One can see that the gain G_{max} decreases with increasing input pulse energies. This is due to inclusion of the nonlinear phenomenon in our model, which leads to the gain saturation effect in the SOA. The value of G_{min} corresponds to the SOA's gain after a long sequence of logic '1' bits. It can be seen that the gain cannot be recovered to its initial value; therefore, the SOA's gain gradually decreases.

To obtain the optimum peak power and the generated FWM signal energy at the SOA output for logic '1' we should analyse the pattern effect and the SOA's gain accurately.

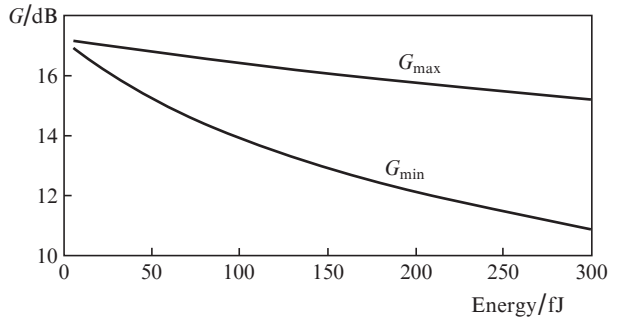

Figure 6. Gain of the SOA vs. the input signal (pump/probe) energy characteristics.

According to the results of Figs 5 and 6, the input energies less than 50 fJ are desirable for obtaining a reasonable PE and SOA gain. Therefore, we use the 40-fJ input energy for the input pump and probe signals at a bit rate of 50 Gb s^{-1}.

Figure 7 shows the simulation results of our proposed all-optical AND logic gate. Figures 7a and b present the data streams for data signal 1 and data signal 2, respectively. The corresponding RZ bit sequences are '1110101101101011' and '1010001011001110' for two input signals (pump and probe pulses). The demodulated bit sequences in Fig. 7c is '1010001001001010', that is equal to the AND logic gate operation between the two input signals (pump and probe pulses).

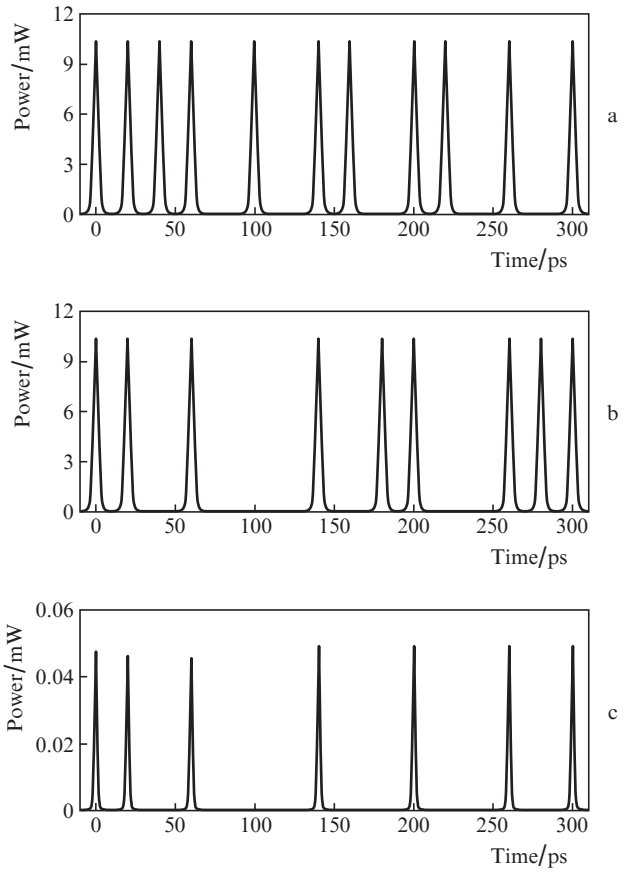

Figure 7. Waveforms for (a) the input serial signal 1, (b) the input serial signal 2, (c) the output FWM signal.

5. Conclusions

Thus, an all-optical AND logic gate using FWM in the SOA is numerically simulated by the FD-BPM technique. For implementing the AND logic gate, all nonlinear parameters such as CD, CH, SHB, GVD, SPM, and TPA are taken into account for modelling. It has been shown that the gain recovery phenomena play an important role for optimising the PE on FWM bit streams. Moreover, although the output FWM signal energy is proportionally related to the input pump and probe signals, for the optimum optical gate operation input signals' energies should be selected, such that the PE is minimal. Therefore, for the 40-fJ input pulse energy, the output FWM signal peak power approximately remains unchanged (0.045 mW) for 50-Gb s^{-1} optical AND logic gate operation.

References

1. Kim S.H. et al. *Proc. 6th Int. Conf. on Numerical Simulation of Optoelectronic Devices 2006 (NUSOD'06)* (Singapore, 2006, pp 91, 92).
2. Han Liu-Yan, Wen He, Jiang Huan, Guo Yi-Li, Zhang Han-Yi. *Chin. Phys. Lett.*, **25** (11), 3901 (2008).
3. Kumar S., Willner A.E. *Opt. Express*, **14** (12), 5092 (2006).
4. Pei-li Li, De-xiu Huang, Xin-liang Zhang, Guang-xi Zhu. *Opt. Express*, **14** (24), 11839 (2006).
5. Dong H., Sun H., Wang Q., Dutta N.K., Jaques J. *Opt. Commun.*, **265** (1), 79 (2006).
6. Li Z. et al. *Electron. Lett.*, **41** (25), 1397 (2005).
7. Zhang X., Wang Y., Sun J., Liu D., Huang D. *Opt. Express*, **12** (3), 361 (2004).
8. Ye L., Hu W., He H. *Proc. 15th Opto-Electronics and Communications Conference (OECC)* (Sapporo, 2010) pp 194, 195.
9. Ibrahim T.A. et al. *IEEE J. Photon. Technol. Lett.*, **15** (10), 1422 (2003).
10. Xu J., Zhang X., Dong J., Liu D., Huang D. *Proc. SPIE Int. Soc. Opt. Eng.*, **6782**, 678209 (2007).
11. Hong M.Y., Chang Y.H., Dienes A., Heritage J.P., Delfyett P.J., Dijaili S., Peterson F.G. *IEEE J. Sel. Top. Quantum Electron.*, **2**, 523 (1996).
12. Das N.K., Yamayoshi Y., Kawaguchi H. *IEEE J. Quantum Electron.*, **36**, 1184 (2000).
13. Razaghi M., Ahmadi V., Connelly M.J. *J. Lightwave Technol.*, **27** (15), 3162 (2009).
14. Hosseini S.R., Razaghi M., Das N.K. *J. Opt. Laser Technol.*, **44**, 528 (2012).
15. Razaghi M., Ahmadi V., Connelly M.J. *Opt. Quantum Electron.*, **41** (7), 513 (2009).
16. Xu J., Zhang X., Mørk J. *IEEE J. Quantum Electron.*, **46** (1), 87 (2010).